



**HAL**  
open science

## Synthesis, structural and magnetic properties of cadmium substituted Li-ferrite

Rulan Verma, Shashank Kane, Priyanka Tiwari, S S Modak, Frédéric  
Mazaleyrat

► **To cite this version:**

Rulan Verma, Shashank Kane, Priyanka Tiwari, S S Modak, Frédéric Mazaleyrat. Synthesis, structural and magnetic properties of cadmium substituted Li-ferrite. *Advances in basic Science (ICABS 2019)*, Feb 2019, Bahal, India. pp.160006, 10.1063/1.5122587. hal-04453297

**HAL Id: hal-04453297**

**<https://hal.science/hal-04453297>**

Submitted on 12 Feb 2024

**HAL** is a multi-disciplinary open access archive for the deposit and dissemination of scientific research documents, whether they are published or not. The documents may come from teaching and research institutions in France or abroad, or from public or private research centers.

L'archive ouverte pluridisciplinaire **HAL**, est destinée au dépôt et à la diffusion de documents scientifiques de niveau recherche, publiés ou non, émanant des établissements d'enseignement et de recherche français ou étrangers, des laboratoires publics ou privés.

Copyright

RESEARCH ARTICLE | AUGUST 29 2019

## Synthesis, structural and magnetic properties of cadmium substituted Li-ferrite

R. Verma; S. N. Kane ; P. Tiwari; S. S. Modak; F. Mazaleyrat

 Check for updates

AIP Conf. Proc. 2142, 160006 (2019)

<https://doi.org/10.1063/1.5122587>



View  
Online



Export  
Citation

CrossMark



Cut Hall measurement time in *half*  
using an M91 FastHall™ controller



Also available as part of a tabletop system and an option for your PPMS® system

# Synthesis, Structural and Magnetic Properties of Cadmium Substituted Li-Ferrite

R. Verma<sup>1</sup>, S. N. Kane<sup>1, a)</sup>, P. Tiwari<sup>1,2</sup>, S. S. Modak<sup>3</sup> and F. Mazaleyrat<sup>4</sup>

<sup>1</sup>Magnetic Materials Laboratory, School of Physics, D. A. University, Khandwa road, Indore – 452001, India.

<sup>2</sup>Department of Physics, Prestige Institute of Engineering Management and Research, Indore - 452010, India.

<sup>3</sup>Physics Department, Jaypee University of Engineering and Technology, Raghogarh, Guna 473226, India.

<sup>4</sup>SATIE, ENS Universite Paris-Saclay, CNRS 8029, 61 Av. du Pdt. Wilson, F-94230, Cachan, France.

<sup>a)</sup>Corresponding author: kane\_sn@yahoo.com

**Abstract.** We present study of  $\text{Li}_{0.5-x/2}\text{Cd}_x\text{Fe}_{2.5-x/2}\text{O}_4$  (thermally treated at 450 °C for 3 hours) nano crystalline ferrites, synthesized by sol-gel auto-combustion method. X-ray diffraction (XRD), magnetic measurements were used to probe the structural, magnetic properties. Results show that successive  $\text{Cd}^{2+}$  addition leads to: i) formation of nano-crystalline phase (Williamson-Hall grain diameter  $D_{W-H}$  range between 16.0 nm – 63.6 nm). Slight presence of  $\alpha\text{-Fe}_2\text{O}_3$  phase was also observed, ii) changes in experimental lattice parameter  $a_{\text{exp}}$  (range between 0.8321 nm – 0.8373 nm), obtained cell volume ( $V$ ), specific surface area ( $S$ ), X-ray density ( $\rho_{\text{XRD}}$ ), are ascribed to the difference in ionic radii of  $\text{Fe}^{3+}$ ,  $\text{Cd}^{2+}$ ,  $\text{Li}^{1+}$  ions; and  $\text{Cd}^{2+}$  ions migrate predominantly to A-site (thus pushing  $\text{Fe}^{3+}$  ions on B site) leading to increased distortion in the lattice displayed by increase of oxygen parameter ( $u$ ) from 0.3797 to 0.3849, iii) migration of cations leads to changes in saturation magnetization  $M_s$  (varies between 52.7 Am<sup>2</sup>/kg – 61.7 Am<sup>2</sup>/kg), whereas coercivity  $H_c$  varies between 111.09 Oe – 150.04 Oe, iv) formation of softer magnetic material with minimum losses of 1.61 J/kg, v) linear variation of  $H_c$  with grain diameter, reveals that the studied samples lie in the region with overlap between single or multi-domain region. Current study clearly shows strong correlation between structural, magnetic properties.

## INTRODUCTION

Spinel ferrites are represented by the formula  $\text{A}^{2+}\text{B}^{3+}_2\text{O}_4$ , where A (tetrahedral), and B (octahedral) sub-lattices form cubic structure, with oxygen anions occupying face centered cubic (fcc) positions. Their structural, magnetic properties can be modified through suitable substitution of divalent cations [1]. Tuning of structure, magnetic properties can be achieved via: partial or complete substitution; a particular synthesis method; thermal treatment etc. Ferrites find applications in various fields including those in permanent magnets, high density storage devices, and targeted drug delivery etc. [2]. It is remarkable to note that a substitution of a magnetic or a non-magnetic cation modifies the cationic distribution on A, B site, and thus would affect the magnetic interactions, which in-turn will influence the magnetic properties [3]. Lithium ferrite is an exclusive member of the spinel group of ferrimagnetic oxides, and has applications in the field of microwave devices because of its square hysteresis loop characteristics, high curie temperature, low microwave dielectric losses, and high saturation magnetization. Literature reports Li–Cd [2], Li–Zn [3], Li–Mg [4], Li–Ni [5] ferrite systems synthesized by different methods (e.g. – double sintering ceramic method, microwave combustion method etc.). Li–Cd ferrites are also important for their applications in isolators, circulators and phase-shifters gyrators [2-5].  $\text{Cd}^{2+}$  ions have preference to occupy A-site, so they would push  $\text{Fe}^{3+}$  ions to B-site, leading to enhancement of magnetic moment, so successive addition of  $\text{Cd}^{2+}$  ions opens-up the possibility of tuning magnetic properties. It is worth noting that in general sintering is needed not only for the formation of spinel phase, but it also improves crystallinity, and helps in achieving equilibrium cationic distribution. A constraint with Li-Cd ferrite is that due to low melting point of both Li and Cd (ranging between 180 – 320 °C), high temperature sintering cannot be used due to evaporation of Li, affecting the stoichiometry. To overcome this constraint, an appropriate synthesis method needs to be used, where either lower sintering temperature or even no sintering can facilitate the formation of spinel phase.

Sol-gel auto combustion synthesis route is of significant relevance, where synthesis is done at relatively lower temperature  $\sim 110$  °C, which also has the advantage of energy efficient synthesis where spinel phase is formed without sintering. Although literature reports Li-Cd based ferrites, however their synthesis via sol-gel auto-combustion method is less-explored in the literature. Hence, in the present work we report our efforts to investigate the structural, magnetic properties of cadmium doped lithium ferrite using sol-gel auto-combustion method, probed through x-ray diffraction (XRD), magnetic measurements.

$I_{hkl}^{obs}$

## EXPERIMENTAL DETAILS, AND DATA ANALYSIS

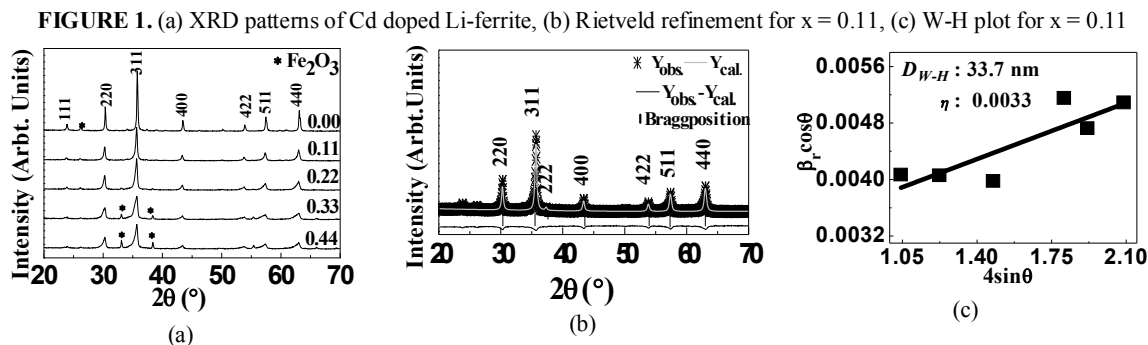
$\text{Li}_{0.5-x/2}\text{Cd}_x\text{Fe}_{2.5-x/2}\text{O}_4$  spinel ferrites were synthesized by sol-gel auto-combustion method as described in [1]. For preparing the samples, in stoichiometric ratio the citrate-nitrate precursors were dissolved in de-ionized water keeping metal salt to citric acid ratio as 1:1, maintaining pH of the solution at 7 by adding ammonia solution ( $\text{NH}_4\text{OH}$ ). Resulting solution was heated at  $\sim 110$  °C to obtain fluffy powder, called ‘as burnt powder’ which was further annealed at 550 °C for 3 hours. Room temperature XRD measurements in  $\theta - 2\theta$  configuration were done by Bruker D8 advance diffractometer utilizing  $\text{CuK}\alpha$  radiation (wavelength: 0.15406 nm). The lattice parameter ( $a_{exp}$ ) was obtained by expression:  $a_{exp} = d\sqrt{h^2 + k^2 + l^2}$  where  $d$  – inter-planer spacing and,  $(h, k, l)$  - miller indices.  $a_{exp}$  was used to obtain the x-ray density ( $\rho_{XRD}$ ) of the studied samples. Particle size ( $D_{W-H}$ ) was obtained by Williamson-Hall (W-H) plot, by incorporating both instrumental, and strain broadening [6]. Specific surface area ( $S$ ) was calculated using the expression:  $S = [6 / (D_{W-H} \times \rho_{XRD})]$ , where  $D_{W-H}$  - particle size and  $\rho_{XRD}$  - x-ray density. Cation distribution of the studied samples was obtained by XRD peak intensities employing Bertaut method [7].

Cation distribution of samples was obtained by using following formula,  $\frac{I_{hkl}^{obs}}{I_{h'k'l}^{obs}} = \frac{I_{hkl}^{cal}}{I_{h'k'l}^{cal}}$ , Where  $I_{hkl}^{obs}$  and  $I_{hkl}^{cal}$  are

observed, and calculated intensities for the reflection (hkl) [8]. Obtained cation distribution was used to calculate, Néel magnetic moment (theoretical magnetization at 0 K ‘ $M_s(0)$ ’), is calculated using formula:  $n_N = M_B - M_A$  in Bohr magneton ( $\mu_B$ ) where  $M_A$  is magnetic moment of A-site and  $M_B$  is magnetic moment of B-site, oxygen position parameter ( $u$ ), ionic radii on A-site ( $r_A$ ) and B-site ( $r_B$ ) and delta parameter ( $\delta$ ). Coercivity ( $H_c$ ), saturation magnetization ( $M_s$ ) and, anisotropy constant ( $K_1$ ), calculated using the expression:  $K_1 = [H_c \times M_s] / 0.96$ , where  $M_s$  – saturation magnetization, static magnetic losses, reduced ramanence were obtained from Hysteresis measurements, were done by Lakeshore VSM Model 7410 by applying maximum field:  $H_{max} \approx \pm 1.9$  T.

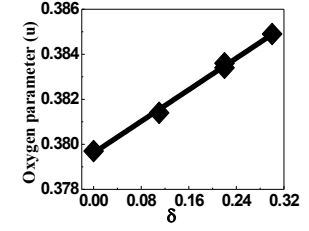
## RESULTS AND DISCUSSIONS

Figure 1 (a), shows the X-ray diffraction pattern of  $\text{Li}_{0.5-x/2}\text{Cd}_x\text{Fe}_{2.5-x/2}\text{O}_4$  nano-ferrite, the existence of the strong diffraction peaks in the annealed powder corresponding to the planes (111), (220), (311), (222), (400), (422), (511), (440), confirms the formation of cubic spinel ferrite with slight presence of  $\alpha\text{-Fe}_2\text{O}_3$  phase was also observed. Figure 1 (b) displays representative Rietveld refined plot for the sample with  $x = 0.11$ , was obtained by material analysis using diffraction (MAUD) software [9]. Representative W-H plot for the sample with  $x = 0.11$  is depicted in figure 1 (c), the analysis of the crystallite size has been carried out using the broadening of XRD peaks. It is known that peak



**Table 1:** Experimental lattice parameter ( $a_{exp}$ ), grain diameter ( $D_{W-H}$ ), cell volume ( $V$ ), x-ray density ( $\rho_{xrd}$ ), specific surface area ( $S$ ) and hopping length for A-site, B-site ( $L_A$ ,  $L_B$ ) and lattice strain ( $\eta$ ) of  $Li_{0.5-x/2}Cd_xFe_{2.5-x/2}O_4$  ferrite.

x	$a_{exp}$ (nm)	$D_{W-H}$ (nm)	V (nm <sup>3</sup> )	S (m <sup>2</sup> /g)	$\rho_{xrd}$ (kg/m <sup>3</sup> )	$L_A$ (nm)	$L_B$ (nm)	$\eta$
0.0	0.8321	63.6	0.5761	29.7	4773.95	0.3603	0.2945	0.0013
0.11	0.8351	33.7	0.5825	42.0	4925.05	0.3616	0.2956	0.0033
0.22	0.8359	26.1	0.5842	53.7	5113.02	0.3619	0.2959	0.0019
0.33	0.8368	16.0	0.5859	81.8	5299.93	0.3623	0.2962	0.0003
0.44	0.8373	18.8	0.5871	632	5491.09	0.3625	0.2964	0.0092



**FIGURE 2.** Variation of  $u$  with  $\delta$ , line connecting points: linear fit to experimental data

broadening results from both finite crystallite size and strain effect within the crystal lattice [10]. Experimental lattice parameter ( $a_{exp}$ ), X-ray density ( $\rho_{XRD}$ ), specific surface area ( $S$ ), cell volume ( $V$ ), hopping length for A-site ( $L_A$ ), B-site ( $L_B$ ) and strain ( $\eta$ ) (of studied samples are depicted in table 1. Lattice parameter (0.8321–0.8373 nm), cell volume (0.5761–0.5871 nm<sup>3</sup>) of Li-Cd ferrite are found to increase with increasing Cd<sup>2+</sup> content are attributed to the replacement of an ion with higher ionic radius (Cd<sup>2+</sup> = 0.097 nm) by smaller ionic radius (Li<sup>1+</sup> = 0.071 nm). X-ray density ( $\rho_{XRD}$ ) increases with increasing Cd<sup>2+</sup> content, attributed to increased molecular weight with substitution of Cd<sup>2+</sup> ions. The behavior of hopping length with Cd content is similar to that of lattice parameter, and this variation is ascribed to the difference in ionic radii of constituent's ions. Obtained values of  $D_{W-H}$  (range between 16.0 nm – 63.6 nm), measured strain ( $\eta$ ) values for the studied samples (range between 0.0013 – 0.0092) are depicted in Table 1.. Observed changes in strain ( $\eta$ ) values are expected to have an effect on magnetic properties. Figure 1 (c), represents W-H plot (*straight line between  $4\sin\theta$  (x-axis) and  $\beta\cos\theta$  (y-axis)*). The slope of the line gives the strain ( $\epsilon$ ) and the intercept ( $0.9\lambda/D$ ) with y-axis gives the crystallite size ( $D$ ) [11].

Cation distribution of mixed Li-Cd ferrite is estimated from XRD intensity ratio, employing Bertaut method. Best information regarding cation distribution can be obtained by comparing experimental and calculated intensity ratios for reflection. This method selects a pairs of reflections calculated intensities for reflection (hkl). In the present study, (220) (422) (440) planes are considered for cation distribution as these planes are sensitive to distribution of cations among tetrahedral  $A$ , octahedral  $B$  sites of the spinel lattice. The calculated, observed intensity ratios were compared for several combinations of cation distribution at A and B-sites. The best cation distribution for tetrahedral and octahedral sites for which, theoretical and experimental intensities ratios agree noticeably are taken to be the accurate one (as described in table 2). A closest agreement between the observed and calculated integrated intensity ratios -  $I_{400/422}$ ,  $I_{220/400}$  (shown in Table 2) suggest that the estimated cation distribution is in good agreement with the real distribution [12].

Perusal of table 2, shows variation of ionic-radii of A-site ( $r_A$ ), B-site ( $r_B$ ), oxygen positional parameter ( $u$ ), delta parameter ( $\delta$ ) with Cd<sup>2+</sup> content. Oxygen position parameter ( $u$ ) increases with increasing content of Cd<sup>2+</sup> can be attributed to migration of Cd<sup>2+</sup> ions to A-site resulting in its expansion. Observed value of oxygen parameter ( $u$ ) increases from 0.3797 to 0.3849, which is slightly greater than its ideal value ( $u_{ideal}$  - 0.375) it could be used as quantitative measurement of oxygen displacement [13]. The inversion parameter ( $\delta$ ) estimated from cation distribution initially shows inverse spinel structure ( $\delta = 0$ ), and with increasing Cd content shows mixed spinel structure ( $\delta = 0.44$ ). Increase of metal ions population (Cd<sup>2+</sup>, Li<sup>1+</sup>) on A-site, there is larger displacement of oxygen anions confirmed in figure 2, where the linear variation of oxygen position parameter ( $u$ ) and delta parameter

**Table 2.** Cation distribution (for A and B site), inversion parameter ( $\delta$ ), oxygen position parameter ( $u$ ), ionic radii on A, B-site ( $r_A$ ,  $r_B$ ), observed, calculated intensity ratios for  $I_{400/422}$ ,  $I_{220/400}$  plane of  $Li_{0.5-x/2}Cd_xFe_{2.5-x/2}$  as a function of Cd<sup>2+</sup> content.

X	Cation distributions	$\delta$	$u_{ideal}$	$r_A$ (nm)	$r_B$ (nm)	$I_{220/400}$		$I_{400/422}$	
						Obs.	Cal.	Obs.	Cal.
0.0	(Fe <sup>3+</sup> <sub>0.5</sub> ) <sup>A</sup> [Li <sup>1+</sup> <sub>0.5</sub> Fe <sup>3+</sup> <sub>1.5</sub> ] <sup>B</sup>	0.00	0.3797	0.0490	0.0835	0.80	0.79	1.22	1.35
0.11	(Cd <sup>2+</sup> <sub>0.11</sub> Fe <sup>3+</sup> <sub>0.89</sub> ) <sup>A</sup> [Li <sup>1+</sup> <sub>0.445</sub> Fe <sup>3+</sup> <sub>1.555</sub> ] <sup>B</sup>	0.11	0.3814	0.0521	0.0831	0.88	0.75	1.31	1.40
0.22	(Li <sup>1+</sup> <sub>0.01</sub> Cd <sup>2+</sup> <sub>0.22</sub> Fe <sup>1+</sup> <sub>0.77</sub> ) <sup>A</sup> [Li <sup>1+</sup> <sub>0.38</sub> Fe <sup>3+</sup> <sub>1.61</sub> ] <sup>B</sup>	0.22	0.3836	0.0554	0.0828	0.95	0.89	1.25	1.31
0.33	(Cd <sup>2+</sup> <sub>0.22</sub> Fe <sup>3+</sup> <sub>0.78</sub> ) <sup>A</sup> [Li <sup>1+</sup> <sub>0.335</sub> Cd <sup>2+</sup> <sub>0.11</sub> Fe <sup>3+</sup> <sub>1.555</sub> ] <sup>B</sup>	0.22	0.3834	0.0553	0.0842	0.76	0.81	1.24	1.31
0.44	(Cd <sup>2+</sup> <sub>0.30</sub> Fe <sup>3+</sup> <sub>0.70</sub> ) <sup>A</sup> [Li <sup>1+</sup> <sub>0.28</sub> Cd <sup>2+</sup> <sub>0.14</sub> Fe <sup>1+</sup> <sub>1.58</sub> ] <sup>B</sup>	0.30	0.3849	0.0577	0.0843	0.84	0.74	1.41	1.52

**Table 3.** Coercivity ( $H_c$ ), experimental saturation magnetization ( $M_s$ ), magnetization at 0K ( $M_{s(0K)}$ ), remanence ( $M_r$ ), squareness ratio ( $M_r/M_s$ ), static magnetic losses and magneto-crystalline anisotropy ( $K_I$ ) of ann.  $\text{Li}_{0.5-x/2}\text{Cd}_x\text{Fe}_{2.5-x/2}\text{O}_4$  ferrite as a function of  $\text{Cd}^{2+}$  content.

X	$H_c$ (Oe)	$M_s$ (Am <sup>2</sup> /kg)	$M_{s(0K)}$ (Am <sup>2</sup> /kg)	$M_r$ (Am <sup>2</sup> /kg)	$M_r/M_s$	Losses (J/kg)	$K_I \times 10^4$ (erg/cc)
0.0	150.04	58.1	134.8	19.14	0.3294	2.4809	4.4286
0.11	132.97	57.7	150.6	17.22	0.2983	2.1094	3.8594
0.22	119.66	61.7	165.6	17.99	0.2917	1.8431	3.8530
0.33	112.53	55.8	164.3	15.06	0.2699	1.6825	3.5185
0.44	111.09	52.7	158.7	14.83	0.2814	1.6102	3.2815

( $\delta$ ). The variation in  $r_A$ ,  $r_B$  values can be attributed to migration of massive  $\text{Cd}^{2+}$  ions on A-site forcing  $\text{Fe}^{3+}$  ions to B site, results in increasing  $u$  value [14].  $\text{Cd}^{2+}$  ions preferentially occupy A-site, while  $\text{Li}^{1+}$  ions are distributed on both A-site and B-sites, because of favorable crystal field effect with increasing Cd content, more fraction of  $\text{Li}^{1+}$  ion become less on tetrahedral site therefore  $\text{Cd}^{2+}$  ions pushes majority of  $\text{Fe}^{3+}$  ions on B-site results in increasing magnetic moment on B-site ( $M = M_B - M_A$ ) up to  $x = 0.22$ , then decreases magnetic moment with increasing  $\text{Cd}^{2+}$  content.

Table 3, shows coercivity ( $H_c$ ), saturation magnetization ( $M_s$ ), remanence ( $M_r$ ), squareness ratio ( $M_r/M_s$ ), and magneto-crystalline anisotropy ( $K_I$ ) values, determined from the M–H curve of the studied Li-Cd ferrite system. Perusal of table 3 shows that  $K_I$  decreases, and thereby  $H_c$  also decreases. Decrease in  $K_I$  can be described in the framework of single ion anisotropy model [15]. According to this model,  $\text{Fe}^{3+}$  ions on A and B sites contribute to anisotropy energy.  $K_I$  is then specified by relative combination of  $\text{Fe}^{3+}$  ions at A site (positive anisotropy) which is compensated by  $\text{Fe}^{3+}$  ions at B site (negative anisotropy). With  $\text{Cd}^{2+}$  doping, cationic re-distribution of  $\text{Fe}^{3+}$  ions yields different concentrations of  $\text{Fe}^{3+}$  ions on A, B sites, and thus affects  $K_I$ . It is noticeable from table 3, that introduction of  $\text{Cd}^{2+}$  into lithium ferrite the magnetic properties are considerably affected.

Figure 3 (a), shows the room temperature hysteresis loop for  $\text{Li}_{0.5-x/2}\text{Cd}_x\text{Fe}_{2.5-x/2}\text{O}_4$  ferrite as a function of  $\text{Cd}^{2+}$  content. This confirms the formation of soft magnetic material with lower hysteresis losses as shown in table 3. In present series an increase of saturation magnetization is observed for  $\text{Cd}^{2+}$  content up to  $x = 0.22$ , and for higher content the saturation magnetization starts to decrease, Neel's two sub lattice model suggests the increase in magnetization is due to strengthening A-B interaction thereafter decreased magnetization is ascribed to modification of exchange interaction in the studied samples. According to Néel two-sub lattice model, theoretical magnetic moment were calculated by using the magnetic moments for  $\text{Cd}^{2+}$ ,  $\text{Li}^{1+}$  and  $\text{Fe}^{3+}$  -  $0\mu_B$ ,  $0\mu_B$ , and  $5\mu_B$  respectively by using equation  $M_{s(t)} = M_B - M_A$

Figure 3 (b), shows similar trend of experimental  $M_s$  at 300 K (obtained from VSM measurements) and that of theoretical magnetization at 0 K:  $M_{s(t)}$  (obtained from cationic distribution, estimated from XRD measurements) shows that the magnetic behavior of the studied annealed samples obeys Néel model [16-17], indicating strong correlation between magnetic, structural properties. Figure 3 (c), shows, the variation of grain diameter ( $D_{W-H}$ ) inset, and shows linear variation of coercivity ( $H_c$ ),

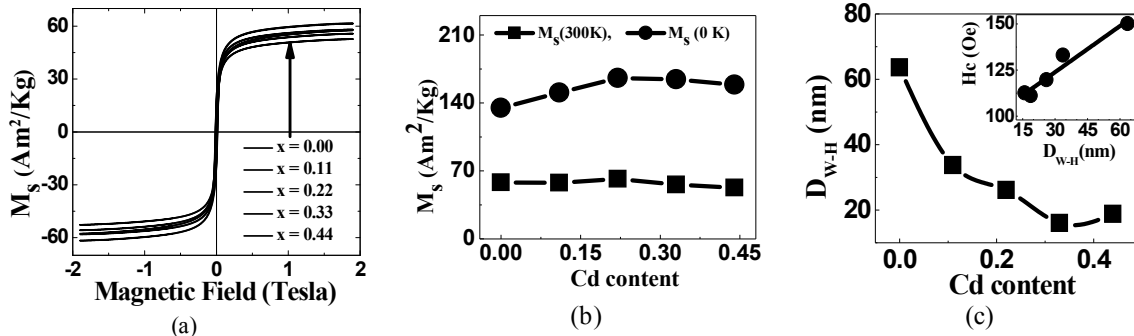


**FIGURE 3.** (a) Hysteresis loops of  $\text{Cd}^{2+}$  doped Li-ferrite (b) Experimental  $M_s$  at 300K, theoretical  $M_{s(t)}$  at 0 K (c) Variation of  $D_{W-H}$  with Cd content. Inset: Variation of ( $H_c$ ) with ( $D_{W-H}$ )

grain size dependence of  $H_c$ . variation of  $H_c$  and  $D_{W-H}$ , in the studied samples lie in the region with overlap between single and multi-domain region as also was suggested earlier [18]. The coercivity of material is related to various factors such as grain size, porosity, nature of cation, and magneto-crystalline anisotropy ( $K_1$ ). Decrease of  $H_c$  can be ascribed to the gradual reduction of magneto-crystalline anisotropy induce by migration of  $Cd^{2+}$  ions from the octahedral site to tetrahedral site. [19-21]. Observed variation in saturation magnetization ( $M_s$ ) with  $Cd^{2+}$  doping is consistent with observed changes in cationic distribution (shown in Table 2).

## SUMMARY

To summarize sol-gel auto-combustion method was used to synthesize  $Cd^{2+}$  doped Li-ferrite. XRD reveals the formation of spinel structure. Grain diameter ( $D_{W-H}$ ) varies between 17.27 – 42.28 nm. Experimental lattice parameter ( $a_{exp}$ ), X-ray density ( $\rho_{XRD}$ ), cell volume ( $V$ ), hopping length for A ( $L_A$ ) and B- ( $L_B$ ) are found to be increase with the increasing content of  $Cd^{2+}$  ascribed to ionic difference of  $Li^{1+}$ ,  $Cd^{2+}$ ,  $Fe^{3+}$ . Cation distribution shows close agreement with real distribution on A and B-sites. The structural parameters such as ionic radii on A-site ( $r_A$ ) and B-site ( $r_B$ ), delta parameter, oxygen position parameters, shared tetrahedral and octahedral edge, unshared octahedral edge changes thus affects the magnetic properties. With increasing  $Cd^{2+}$  content whereas saturation magnetization initially increased till  $x = 0.22$ , thereafter decreases, ascribed to modification of exchange interaction.

## ACKNOWLEDGMENTS

Authors thank Dr. M Gupta, UGC-DAE CSR, Indore for XRD measurements. S. N. Kane acknowledges gratefully one month hospitality as invited professor at Ecole Normale Supérieure de Cachan, University Paris-Saclay (France), during Nov.-Dec. 2017.

## REFERENCES

1. S. S. Bellad, R. B. Pujar, B. K. Chougule, *Materials Chemistry and Physics*, **52**, 166–169 (1998).
2. S. N. Kane, S. Raguwanshi, M. Satalkar, V. R. Reddy, U. P. Deshpande, T. R. Tatarchuk and F. Mazaleyrat, *AIP Conf. Proc.* **1953**, 030089-4 (2018).
3. V. K. Sankaranarayanan, Om Prakasha, R. P. Panta and M. Islam, *J. Magn. Magn. Mater.* **252**, 7–9 (2002).
4. S.C. Watawe, S. Keluskar, Gonbare, R. Tangsali, *Thin Solid Films* **505**, 168–172 (2006).
5. S. Akhter, M. A. Hakim, *Mater. Chem. Phys.* **120**, 399–403 (2010).
6. R. Verma, S. N. Kane, S. Raghuvanshi, M. Satalkar, S. S. Modak and F. Mazaleyrat, *AIP Conf. Proc.* **1953**, 030135-1-030135-4 (2018).
7. L. Gastaldi and A. Lapicciarella, *J. Solid State Chem.* **30**, 223 (1979).
8. E. F. Bertaut, C. R. Acad. Sci. **230**, 213 (1950).
9. L. Lutterotti and P. scardi, *J. Appl. Cryst* **23**, 246-252 (1990).
10. S. K. Nath, K. H. Maria, S. Noor, S. S. Sikder, S. M. Hoque, M. A. Hakim, *J. Magn. Magn. Mater.* **324**, 2116–2120 (2012).
11. T. Tatarchuk, M. Bououdina, W. Macyk, O. Shyichuk, N. Paliychuk, I. Yaremiy, B. Al-Najar and M. Pacia, *Nanoscale Res. Lett.* **12**, 141-11 (2017).
12. J. Smit, H. P. J. Wijn, Ferites, Philips Technical Library, Eindhoven, (1959).
13. S. Raghuvanshi, F. Mazaleyrat, and S. N. Kane, *AIP Advances* **8**, 047804–1-047804-11 (2018).
14. D. R. Mane, S. Patil, D. D. Birajdar, A. B. Kadam, S. Shirsath and R. H. Kadam, *Mater. Chem. Phys.*, **126**, 755–760 (2011).
15. R. G. Kharabe, R. S. Devan, C. M. Kanamadi and B. K. Chougule, *Smart Mater. Strut.* **15**, N36–N39 (2006).
16. S. Panchal, S. Raghuvanshi, K. Gahlot, F. Mazaleyrat and S. N. Kane, *AIP Advances* **6**, 055930–6 (2016).
17. S. N. Kane and M. Satalkar, *J. Mater. Sci.* **52**, 3467–3477 (2017).
18. A. Kolhatkar, A. C. Jamison, D. Litvinov and T. R. Lee, *Int. J. Mol. Sci.* **14(8)**, 15977–16009 (2013).
19. M. M. Hessian, *Journal of Magnetism and Magnetic Materials*, **320**, 2800–2807 (2008).
20. G. Barrera, M. Coisson, F. Celegato, S. Raghuvanshi, F. Mazaleyrat, S. N. Kane and P. Tiberto, *J. Magn. Magn. Mater.*, **456**, 372–380 (2018).
21. A. M. Shaikh, S. S. Bellad and B. K. Chougule, *J. Magn. Magn. Mater.*, **195**, 384–390 (1999).